FeNi alloys embedded in porous carbon shells on dual-substrate as efficient electrocatalyst for zinc-air batteries

Han Guo [a], Guangxu Yao [a], Chuanzhen Feng [a], Mi Wang [a], Huijuan Zhang [*a,b] and Yu Wang [*a,b]

[a] *School of Chemistry and Chemical Engineering, Chongqing University, Chongqing, 400044, P. R. China. E-mail: zhanghj@cqu.edu.cn; wangy@cqu.edu.cn*

[b] *College of Chemistry and Environmental Science, Inner Mongolia Normal University, Huhehaote, 010022, P. R. China*

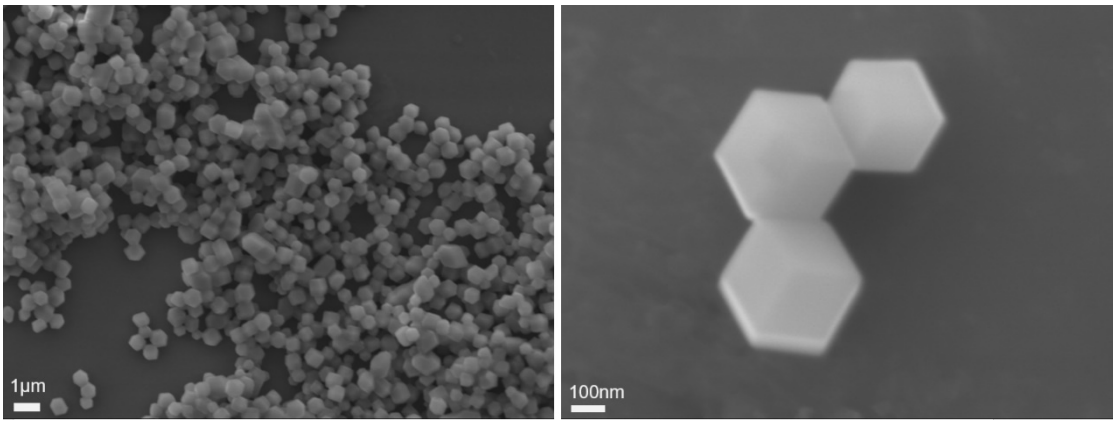

Fig. S1. SEM images of ZIF-8 at different magnifications.

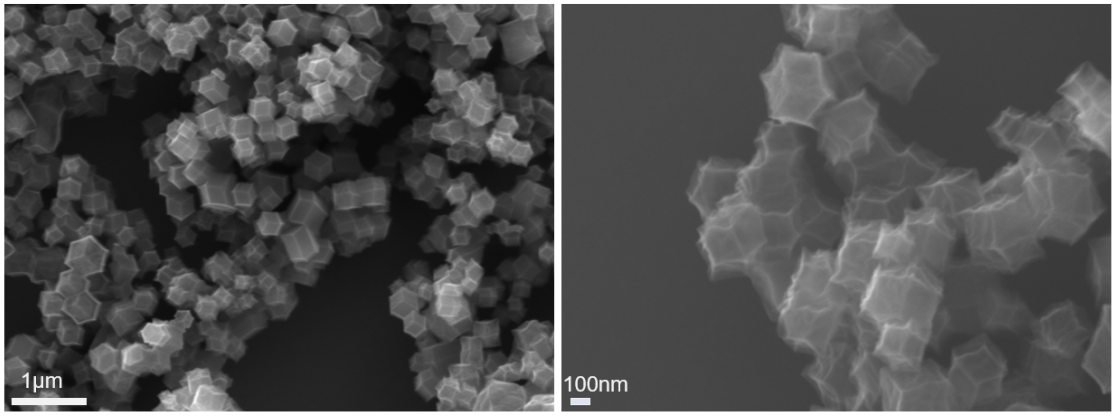

Fig. S2. SEM images of NC at different magnifications.

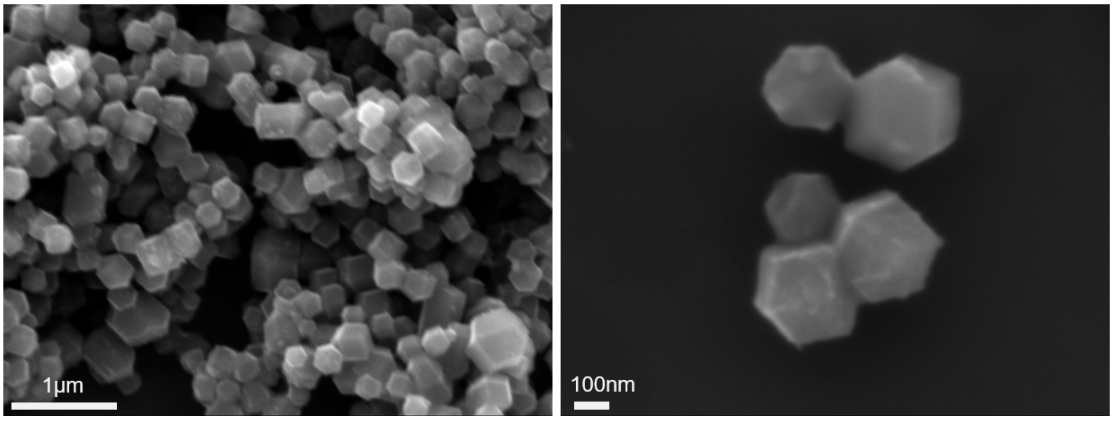

Fig. S3. SEM images of FeNi/NC at different magnifications.

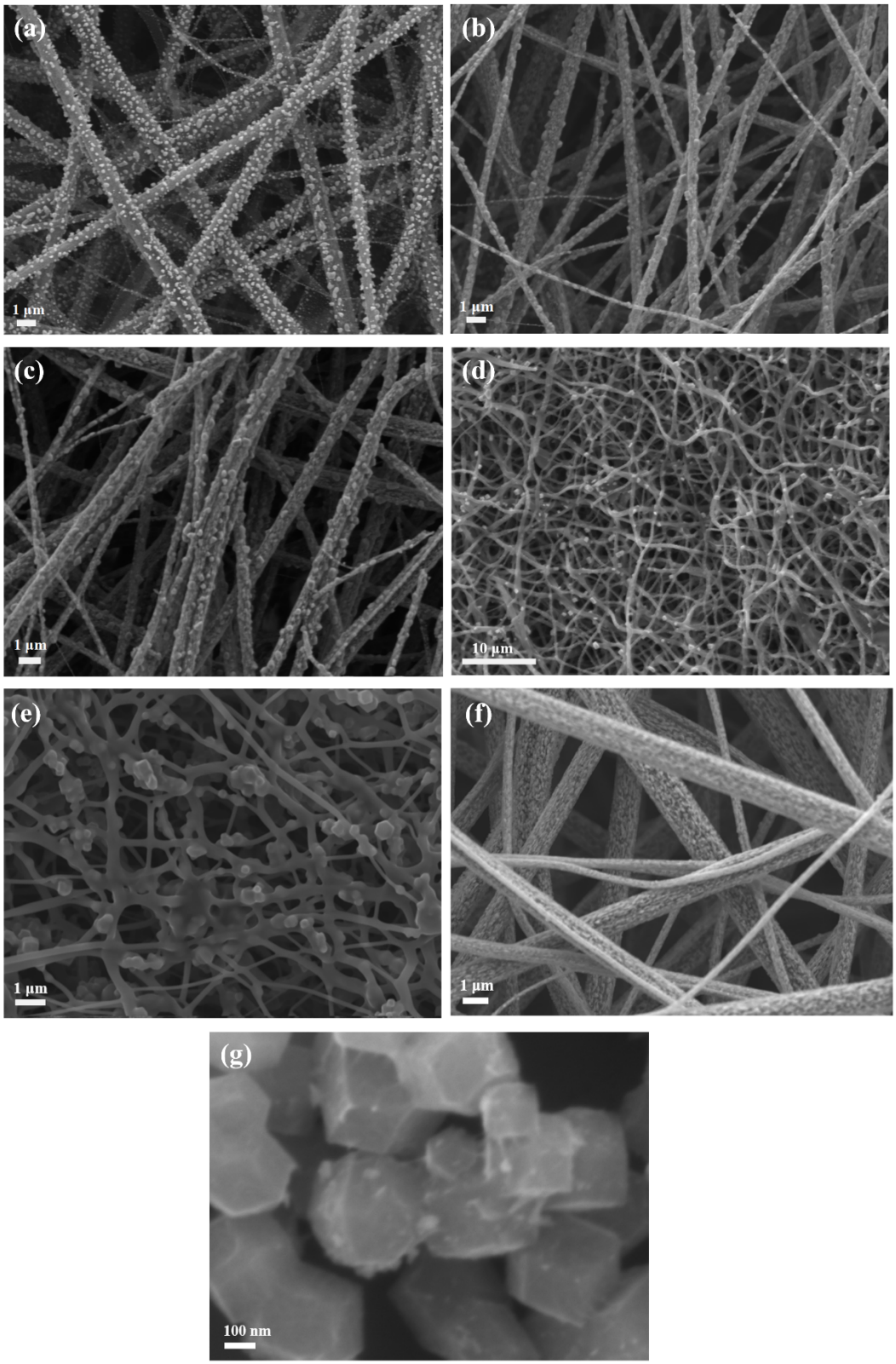

Fig. S4. SEM images of (a) FeNi@Ti_4O_7-CNFs, (b) Ni/NC@Ti_4O_7-CNFs, (c) Fe/NC@Ti_4O_7-CNFs, (d) NC@Ti_4O_7-CNFs, (e) FeNi/NC-CNFs, (f) Ti_4O_7-CNFs and (g) FeNi/NC.

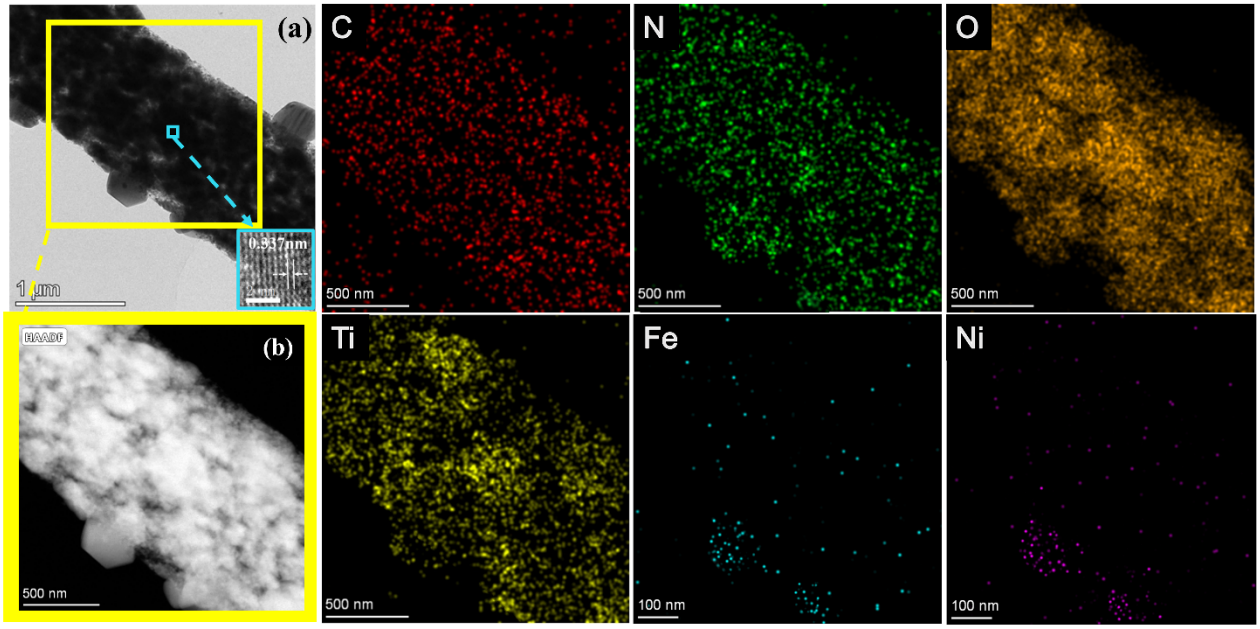

Fig. S5. (a) TEM images of FeNi/NC@Ti_4O_7-CNFs. (a) Inset, dot-matrix striped image of labeled area. (b) HAADF-STEM image, and the corresponding FeNi/NC@Ti_4O_7-CNFs EDS mapped image.

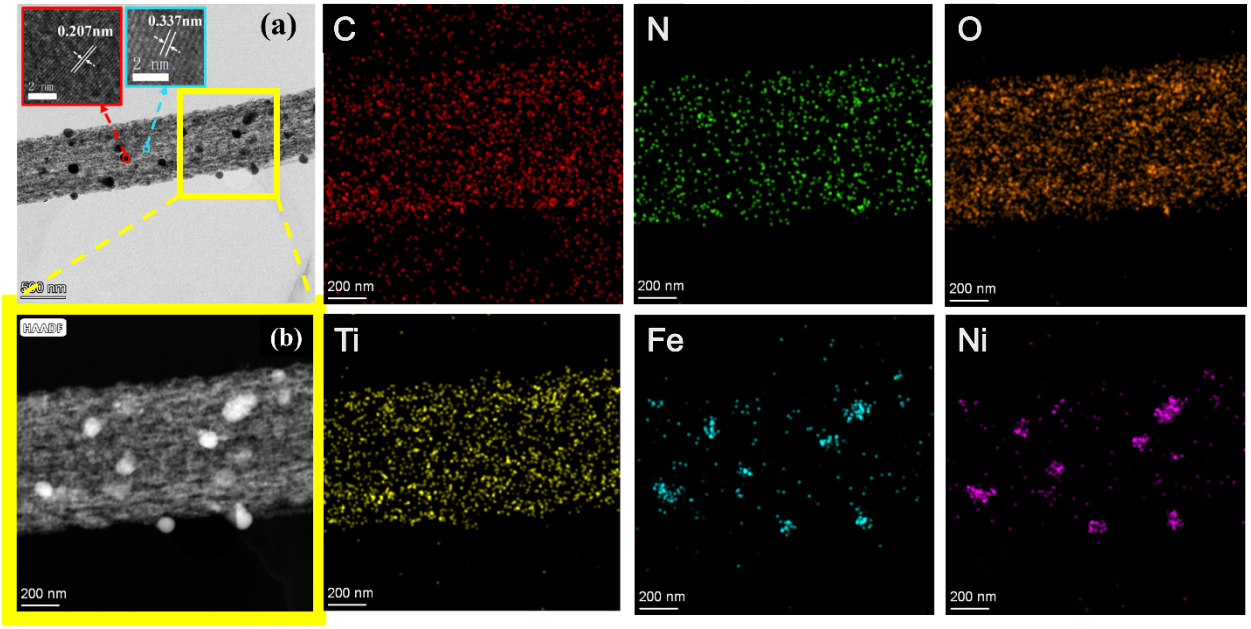

Fig. S6. (a) TEM images of FeNi@Ti_4O_7-CNFs. (a) Inset, dot-matrix striped image of labeled area. (b) HAADF-STEM image, and the corresponding FeNi@Ti_4O_7-CNFs EDS mapped image.

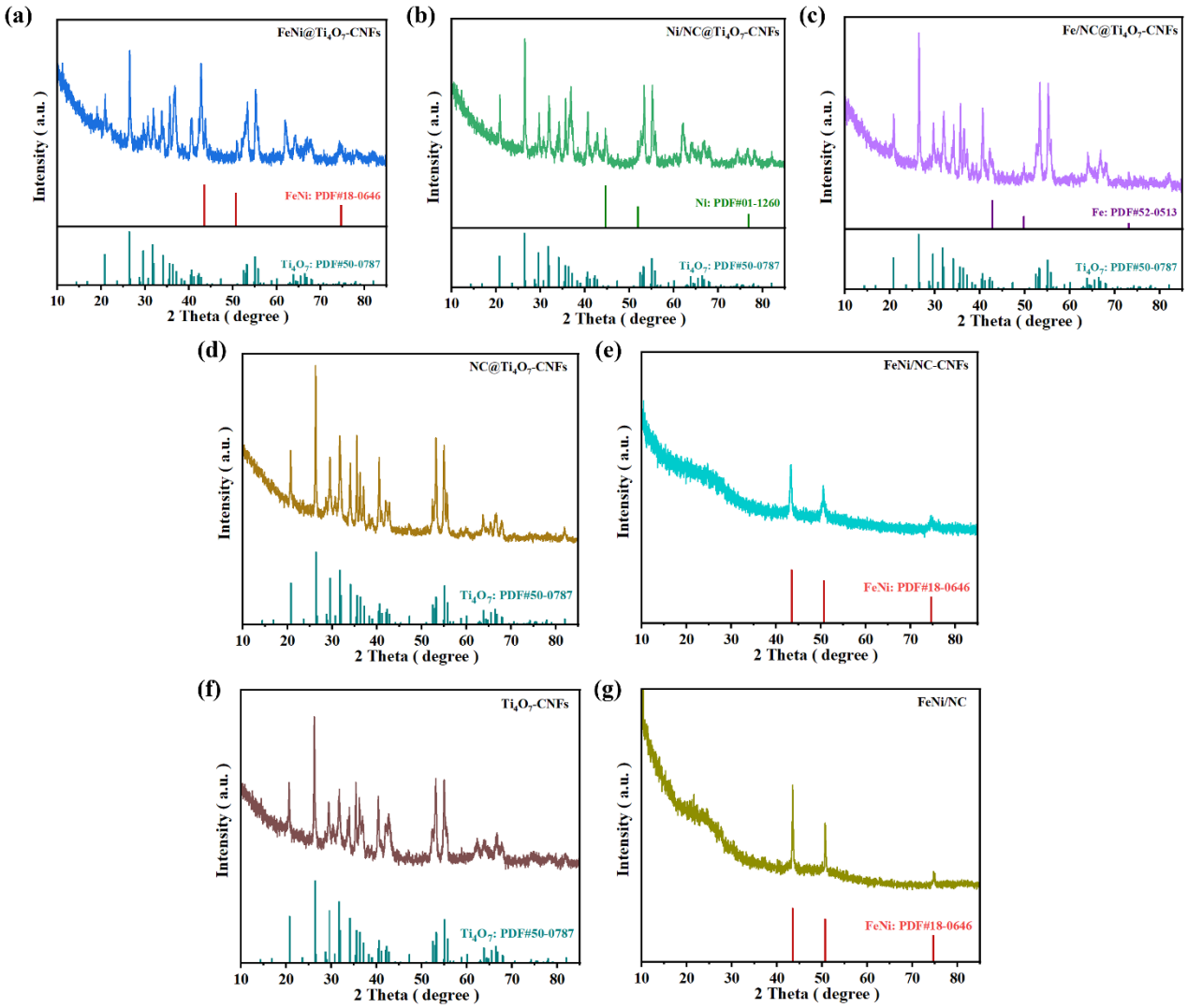

Fig. S7. XRD patterns of (a) FeNi@Ti_4O_7-CNFs, (b) Ni/NC@Ti_4O_7-CNFs, (c) Fe/NC@Ti_4O_7-CNFs, (d) NC@Ti_4O_7-CNFs, (e) FeNi/NC-CNFs, (f) Ti_4O_7-CNFs and (g) FeNi/NC.

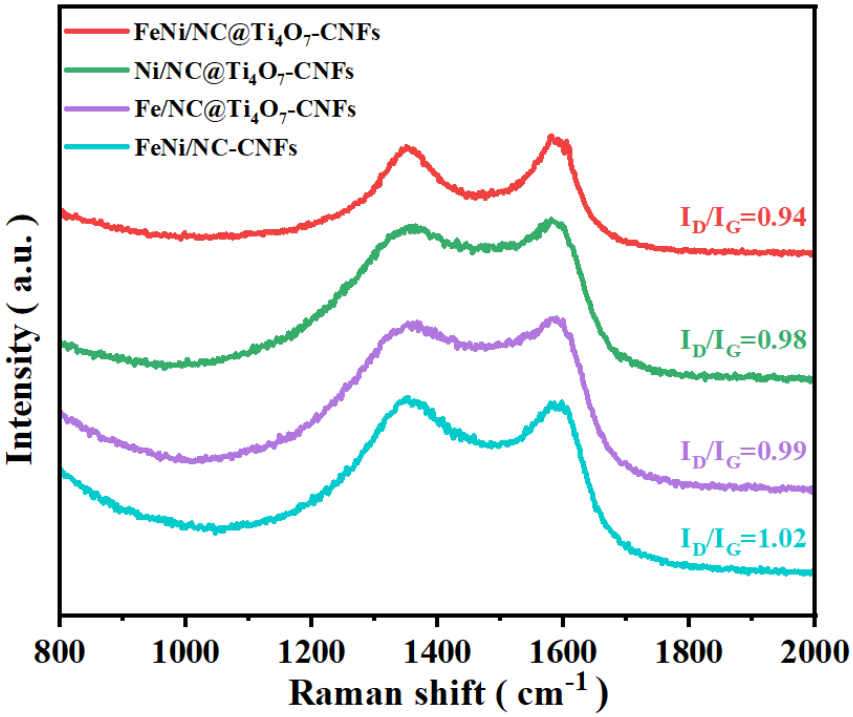

Fig. S8. Raman spectra of Ni/NC@Ti_4O_7-CNFs, Fe/NC@Ti_4O_7-CNFs and FeNi/NC-CNFs.

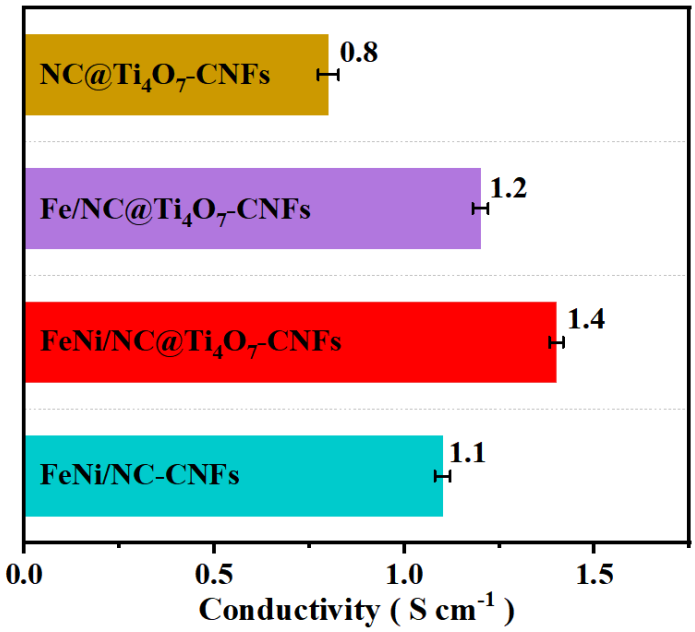

Fig. S9. The conductivity of FeNi/NC-CNFs, FeNi/NC@Ti_4O_7-CNFs, Fe/NC@Ti_4O_7-CNFs and NC@Ti_4O_7-CNFs. Error bars indicate at least three independent measurements of the same catalyst.

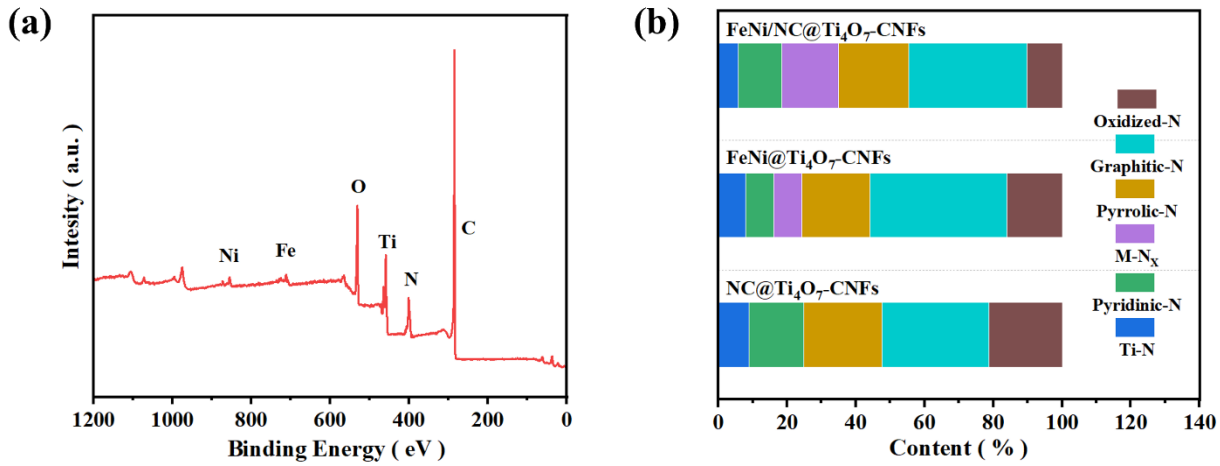

Fig. S10. (a) XPS full measurement spectra of FeNi/NC@Ti_4O_7-CNFs. (b) N content of FeNi/NC@Ti_4O_7-CNFs, FeNi@Ti_4O_7-CNFs and NC@Ti_4O_7-CNFs.

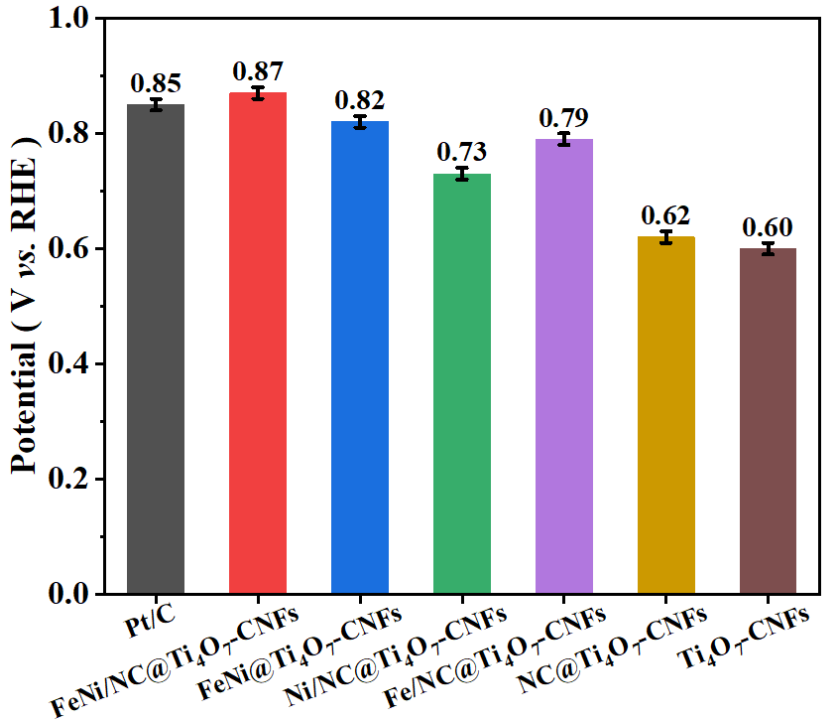

Fig. S11. Comparison of half-wave potentials ($E_{1/2}$) for different catalysts. Error bars indicate at least three independent measurements for the same catalyst.

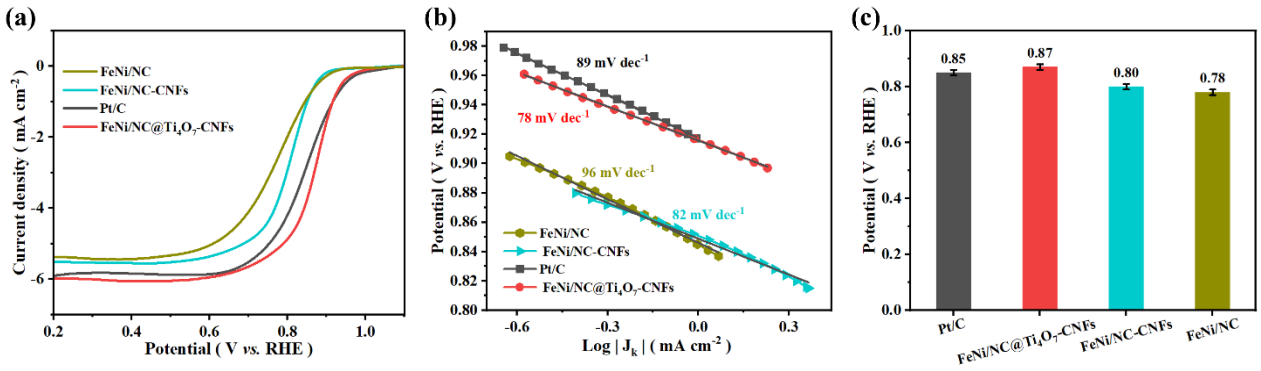

Fig. S12. (a) LSV curve of FeNi/NC-CNFs and FeNi/NC in 0.1 M O_2-saturated KOH solution (1600 rpm). (b) Tafel slope plot. (c) Half-wave potential ($E_{1/2}$). Error bars indicate at least three independent measurements for the same catalyst.

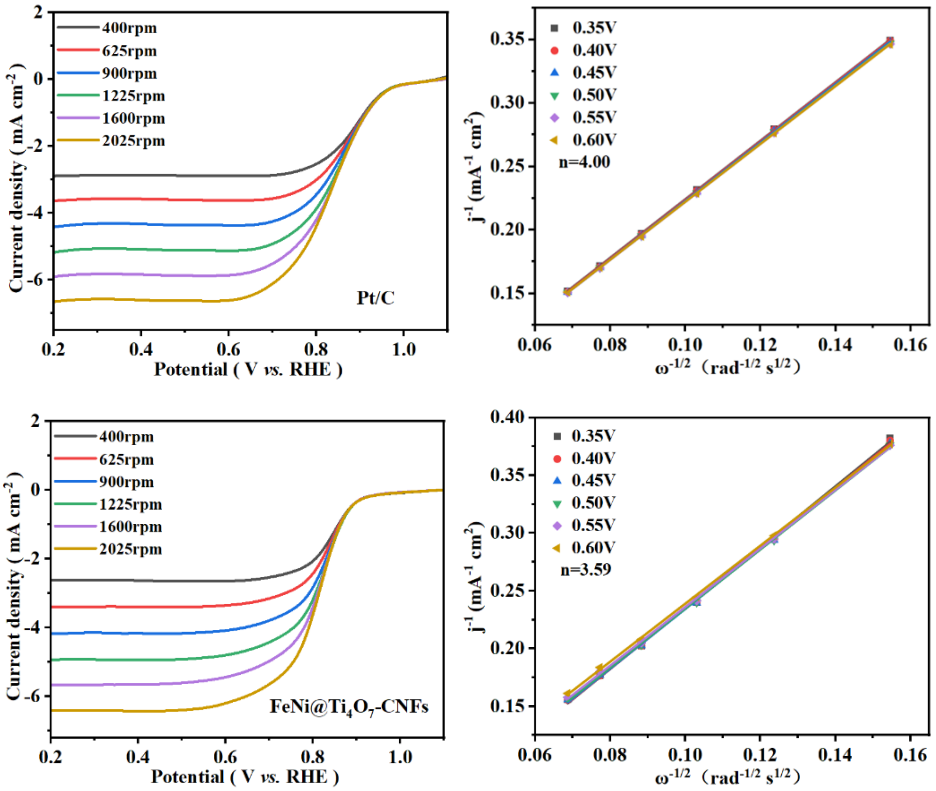

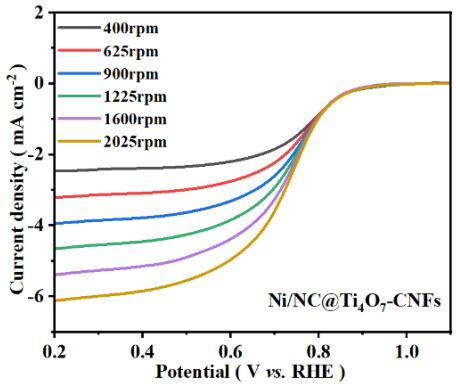
400rpm
625rpm
900rpm
1225rpm
1600rpm
2025rpm
Ni/NC@Ti4O7-CNFs
Current density (mA cm-2)
Potential (V vs. RHE)

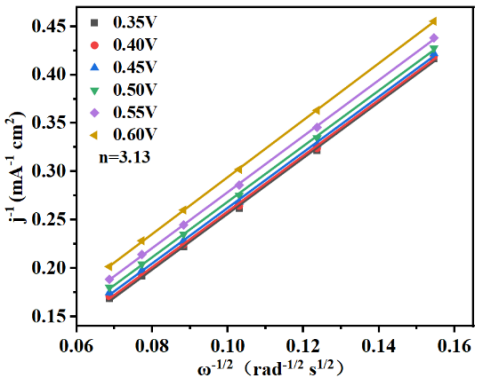
0.35V
0.40V
0.45V
0.50V
0.55V
0.60V
n=3.13
j-1 (mA-1 cm2)
ω-1/2 (rad-1/2 s1/2)

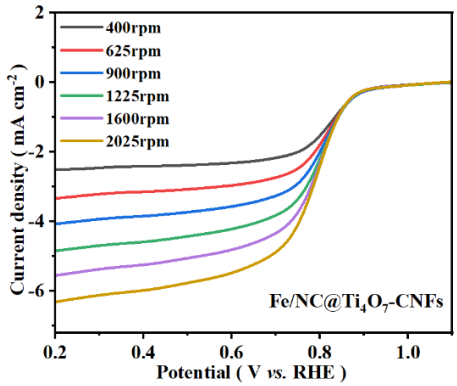
400rpm
625rpm
900rpm
1225rpm
1600rpm
2025rpm
Fe/NC@Ti4O7-CNFs
Current density (mA cm-2)
Potential (V vs. RHE)

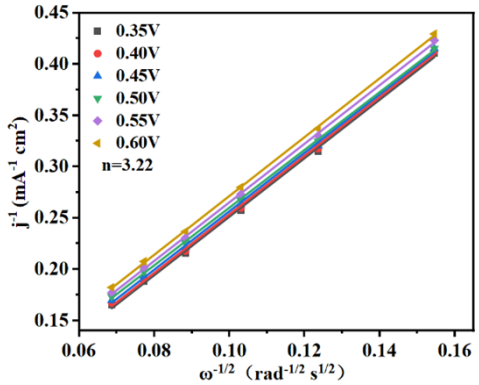
0.35V
0.40V
0.45V
0.50V
0.55V
0.60V
n=3.22
j-1 (mA-1 cm2)
ω-1/2 (rad-1/2 s1/2)

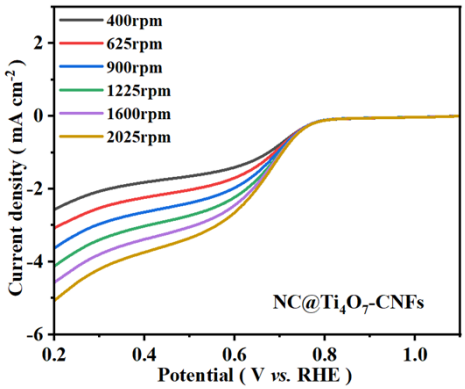
400rpm
625rpm
900rpm
1225rpm
1600rpm
2025rpm
NC@Ti4O7-CNFs
Current density (mA cm-2)
Potential (V vs. RHE)

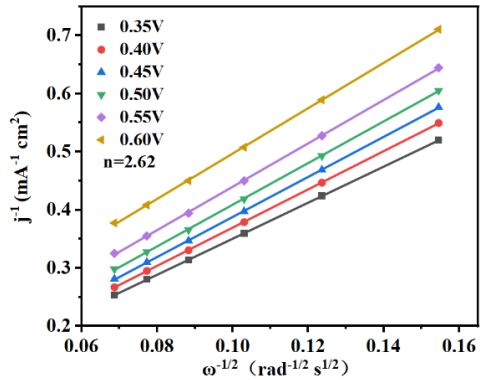
0.35V
0.40V
0.45V
0.50V
0.55V
0.60V
n=2.62
j-1 (mA-1 cm2)
ω-1/2 (rad-1/2 s1/2)

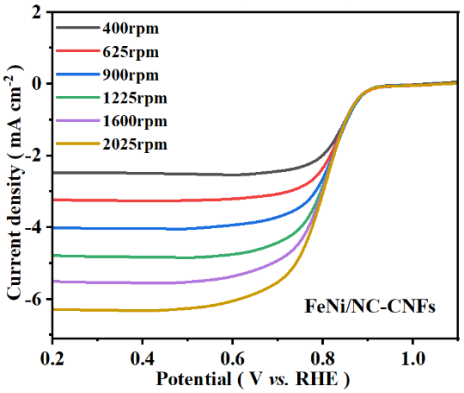
400rpm
625rpm
900rpm
1225rpm
1600rpm
2025rpm
FeNi/NC-CNFs
Current density (mA cm-2)
Potential (V vs. RHE)

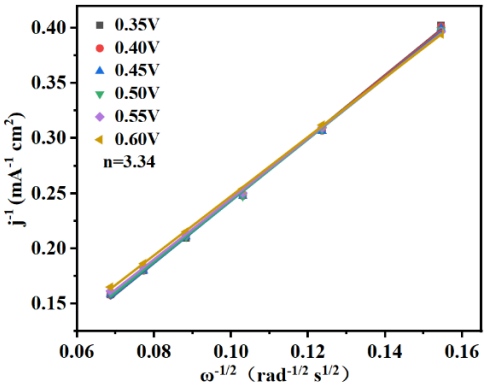
0.35V
0.40V
0.45V
0.50V
0.55V
0.60V
n=3.34
j-1 (mA-1 cm2)
ω-1/2 (rad-1/2 s1/2)

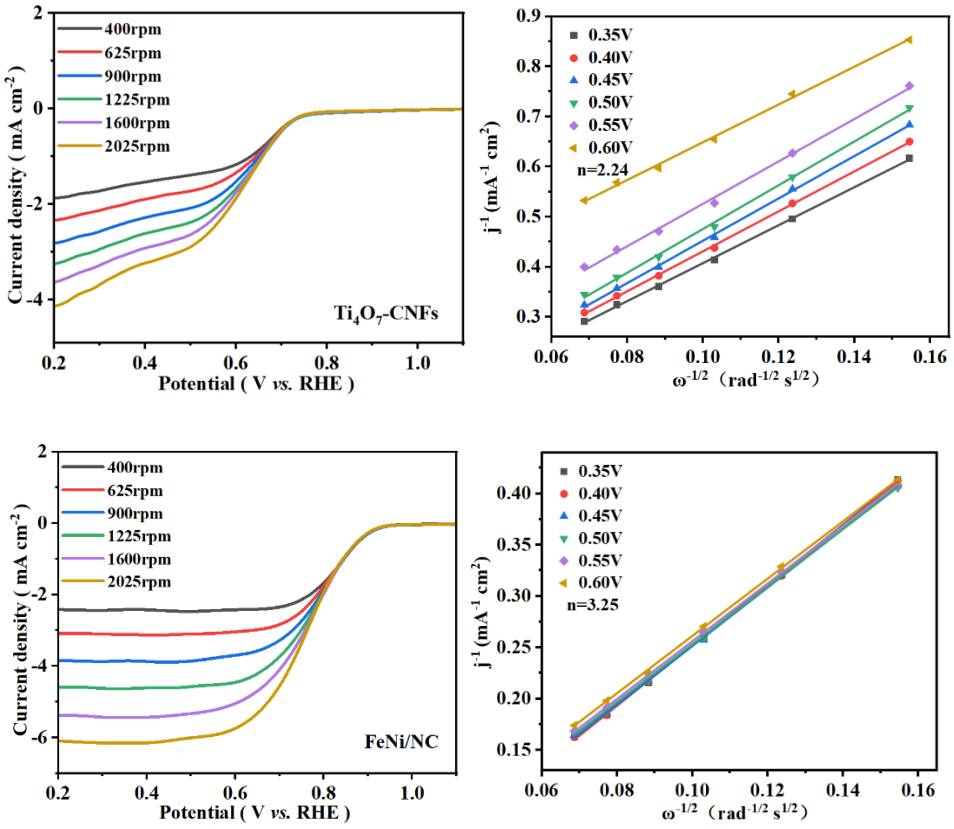

Fig. S13. LSV curves of Pt/C, FeNi@Ti_4O_7-CNFs, Ni/NC@Ti_4O_7-CNFs, Fe/NC@Ti_4O_7-CNFs, NC@Ti_4O_7-CNFs, FeNi/NC-CNFs, Ti_4O_7-CNFs and FeNi/NC in O_2-saturated 0.1 M KOH solution and corresponding Koutecky -Lecich (K-L) plots.

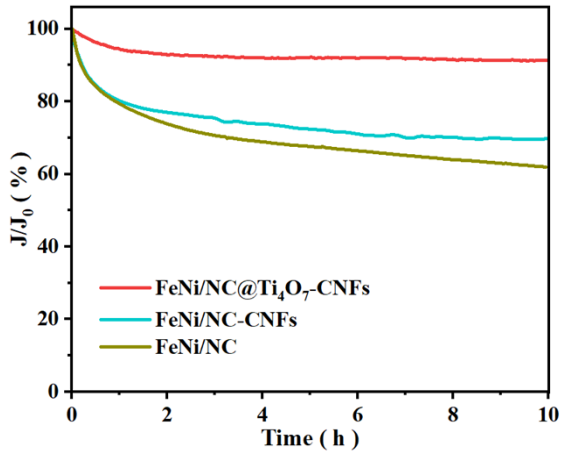

Fig. S14. Endurance test at 1 V (vs. RHE) for FeNi/NC-CNFs and FeNi/NC.

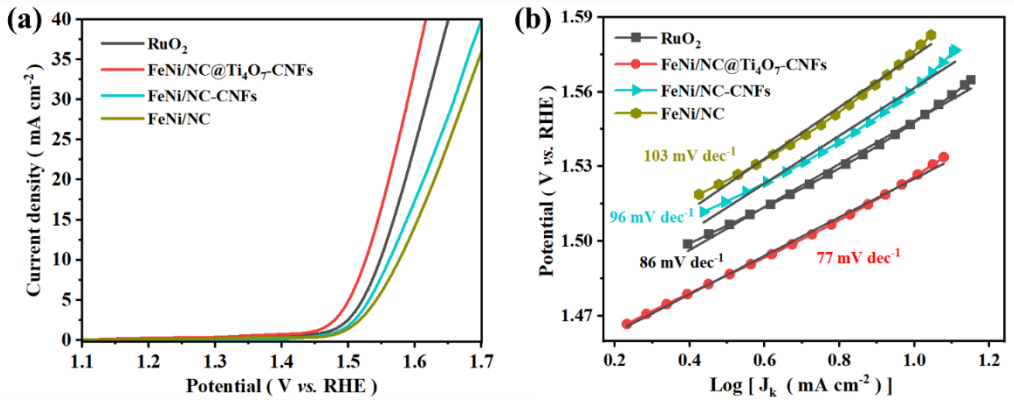

Fig. S15. (a) LSV curves of FeNi/NC-CNFs and FeNi/NC in 1 M KOH solution. (b) Tafel slope plot.

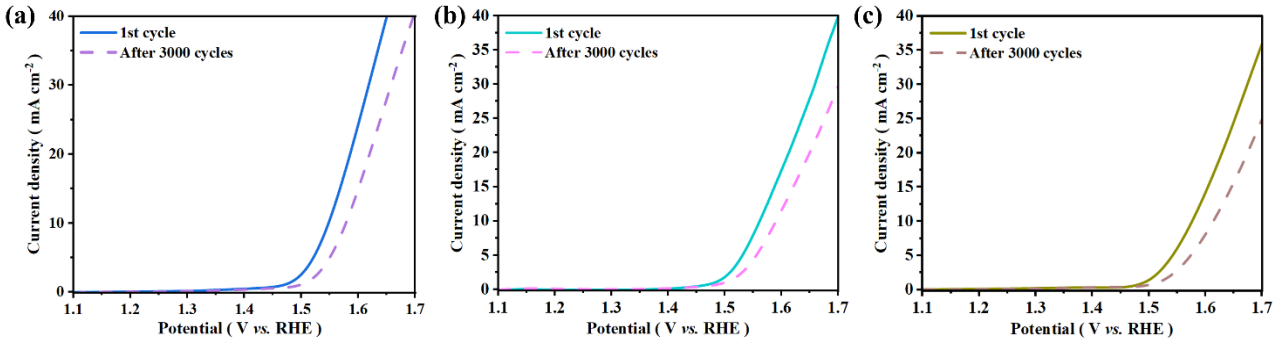

Fig. S16. LSV curves before and after 3000 cycles of (a) RuO_2, (b) FeNi/NC-CNFs and (c) FeNi/NC.

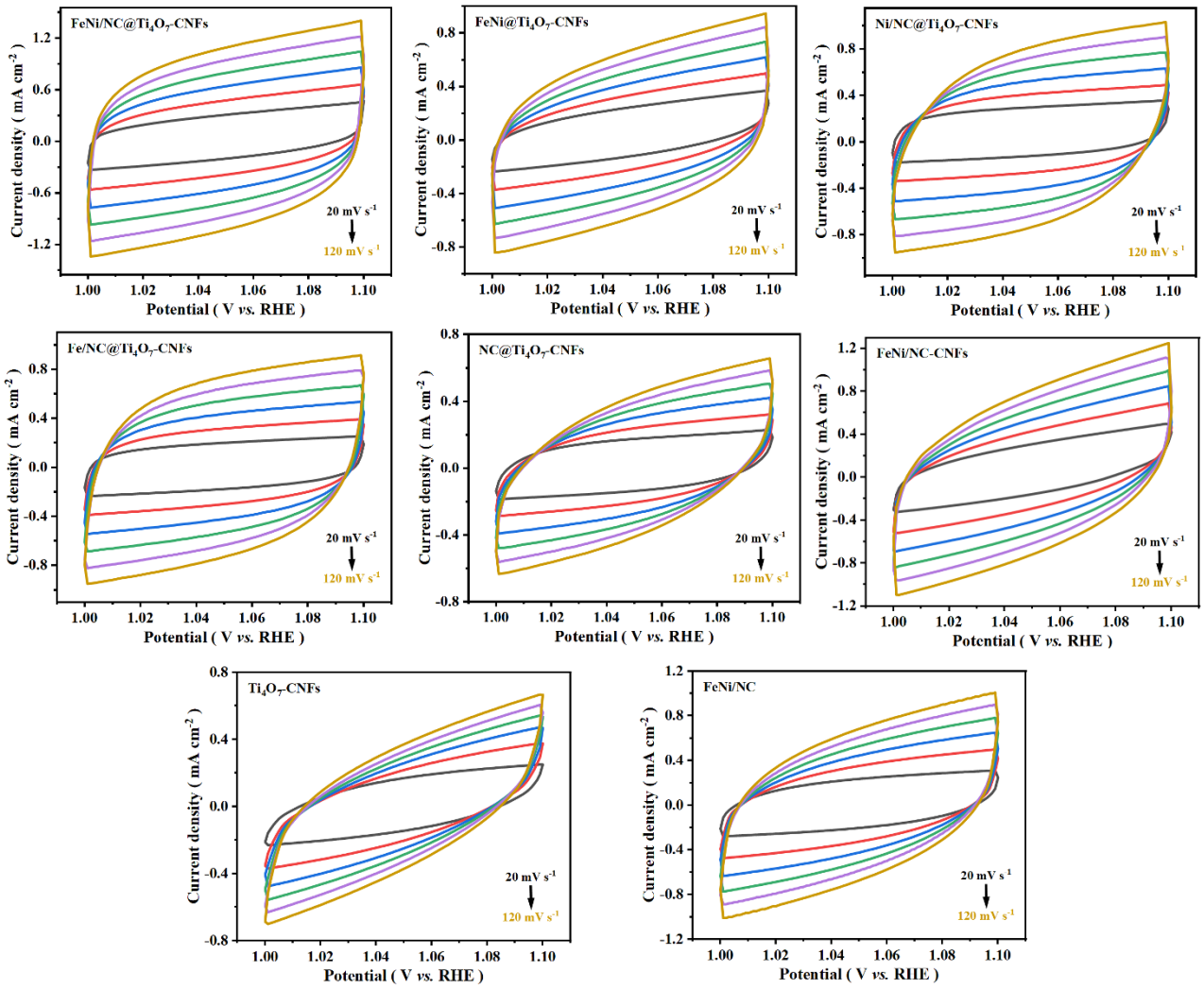

Fig. S17. Capacitance CV curves of FeNi/NC@Ti_4O_7-CNFs, FeNi@Ti_4O_7-CNFs, Ni/NC@Ti_4O_7-CNFs, Fe/NC@Ti_4O_7-CNFs, NC@Ti_4O_7-CNFs, FeNi/NC-CNFs, Ti_4O_7-CNFs and FeNi/NC in the non-Faraday region at different scanning rates.

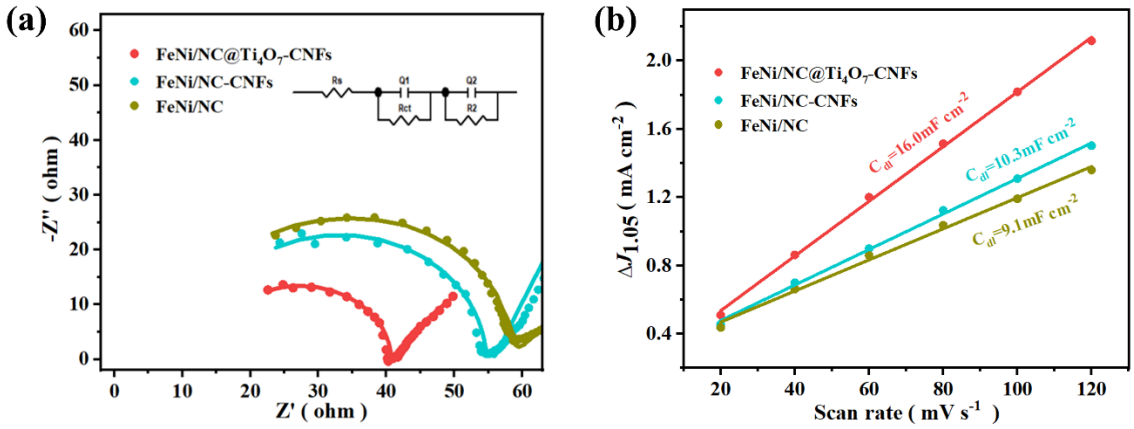

Fig. S18. (a) EIS Nyquist plot of FeNi/NC-CNFs and FeNi/NC; (a) Inset, fitted equivalent

circuit diagram. (b) Capacitance current versus scan rate at 1.05 V to assess the C_{dl} of the catalysts.

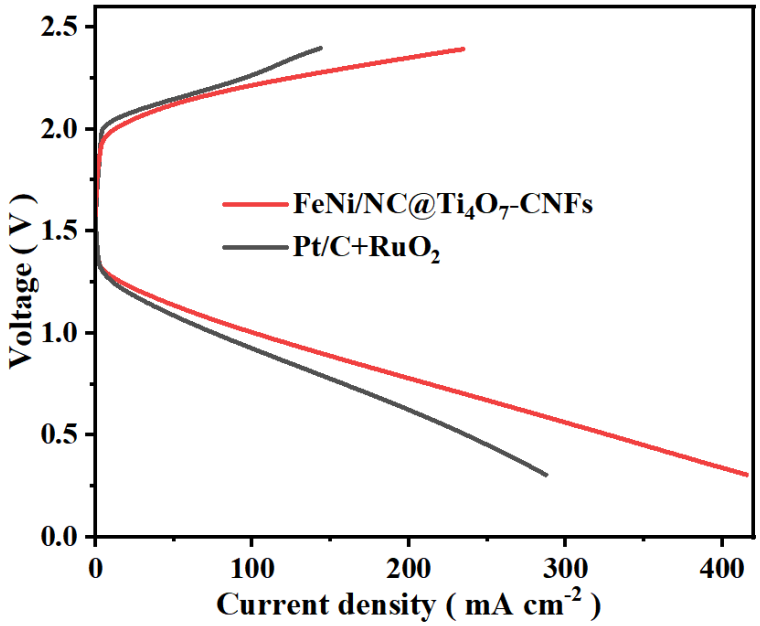

Fig. S19. Charge-discharge polarization curves of liquid ZABs assembled by FeNi/NC@Ti_4O_7-CNFs and Pt/C+RuO_2 hybrid catalysts as air cathodes, respectively.

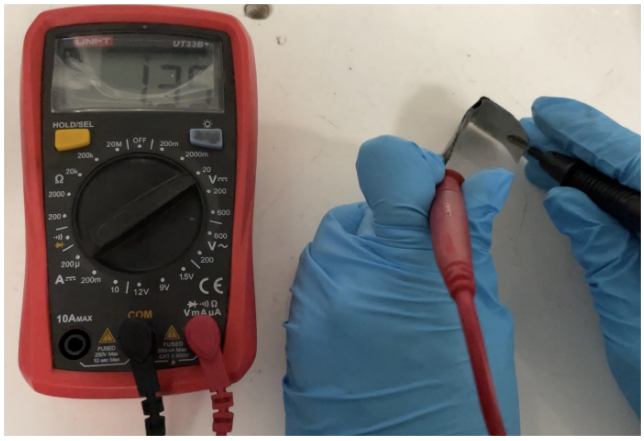

Fig. S20. Photograph of the open-circuit voltage of a flexible solid-state ZAB assembled with FeNi/NC@Ti_4O_7-CNFs as air cathodes under bending conditions.

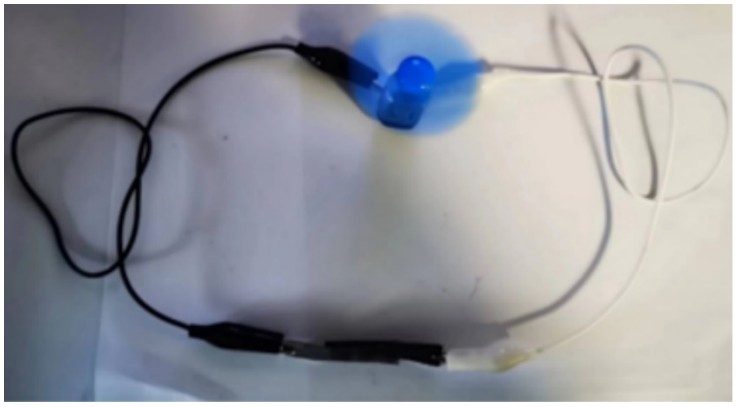

Fig. S21. Photograph of a flexible solid-state ZAB assembled with FeNi/NC@Ti_4O_7-CNFs as air cathodes used in tandem to power a fan.

Table S1. Metal contents of catalysts measured by ICP (at%).

Samples	Fe	Ni
FeNi/NC@Ti_4O_7-CNFs	1.37	1.34
FeNi@Ti_4O_7-CNFs	1.56	1.53
Ni/NC@Ti_4O_7-CNFs	--	2.63
Fe/NC@Ti_4O_7-CNFs	2.68	--

Table S2. Comparison of ORR and OER activities of FeNi/NC@Ti_4O_7-CNFs with other previously reported bifunctional electrocatalysts.

Catalyst	$E_{1/2}$ (V vs. RHE)	$E_{j=10}$ (V vs. RHE)	ΔE (V)	Ref.
FeNi/NC@Ti_4O_7-CNFs	0.87 (0.1 M KOH)	1.526 (1 M KOH)	0.656	This work
NiFe/Fe,N-CB	0.8 (0.1 M KOH)	1.511 (1 M KOH)	0.71	[1]
Fe–NiNC-50	0.84 (0.1 M KOH)	1.57 (1 M KOH)	0.73	[2]

NiFe@C@Co CNFs	0.87 (0.1 M KOH)	1.6 (1 M KOH)	0.73	3
$Fe_{0.5}Ni_{0.5}$@N-GR	0.69 (0.1 M KOH)	1.44 (1 M KOH)	0.75	4
$FeNi_3$@NC	0.783 (0.1 M KOH)	1.522 (1 M KOH)	0.739	5
NiFe/Co-N@CNTs	0.87 (0.1 M KOH)	1.53 (1 M KOH)	0.66	6
$FeNi_3C_x$-Pd-7%	0.80 (0.1 M KOH)	1.518($E_{j=50}$) (1 M KOH)	--	7
FeNi/NC	0.807 (0.1 M KOH)	1.576 (1 M KOH)	0.769	8
FeNi@N-CNT/NCS	0.84 (0.1 M KOH)	1.59 (1 M KOH)	0.75	9
FeNiCo@NC-P	0.84 (0.1 M KOH)	1.54 (0.1 M KOH)	0.70	10
NiFe/N-CNT	0.75 (0.1 M KOH)	1.52 (0.1 M KOH)	0.77	11
Fe-Co-Ni MOF	0.75 (0.1 M KOH)	1.48 (1 M KOH)	0.73	12

Table S3. Comparison of the performance of liquid ZABs assembled with FeNi/NC@Ti_4O_7-CNFs with other previously reported bifunctional electrocatalysts.

Catalyst	**OCV (V)**	**Power density (mW cm^{-2})**	**Specific capacity (mAh·g_{Zn}^{-1})**	**Cycling stability**	**Ref.**
FeNi/NC@Ti_4O_7-CNFs	1.52	169.5	802.6 (5 mA cm^{-2})	320 hours / 960cycles (5 mA cm^{-2})	This work
NiFe/Fe,N-CB	1.565	66	731.0 (5 mA cm^{-2})	280 cycles (5 mA cm^{-2})	1
Fe–NiNC-50	1.41	220	752.14 (5 mA cm^{-2})	100 hours (2 mA cm^{-2})	2
NiFe@C@Co CNFs	1.44	130	694.0 (5 mA cm^{-2})	200 hours (5 mA cm^{-2})	3

$Fe_{0.5}Ni_{0.5}$@N-GR	1.482	85	940 (5 mA cm^{-2})	40 hours (20 mA cm^{-2})	4
$FeNi_3$@NC	1.48	149.7	658 (10 mA cm^{-2})	280 hours (5 mA cm^{-2})	5
FeNiCo@NC-P	1.36	112.0	807 (10 mA cm^{-2})	130 hours / 130 cycles (10 mA cm^{-2})	13
NiFe@N-CFs	1.40	102	719 (5 mA cm^{-2})	100 hours / 300 cycles (10 mA cm^{-2})	14
Ni_3Fe/Co-N-C	1.39	68	--	65 hours (10 mA cm^{-2})	15
FeNi@NC	1.49	98	649 (10 mA cm^{-2})	240 hours (10 mA cm^{-2})	16
FeNi–N–C@FeNi LDH	1.497	73.9	749.3 (10 mA cm^{-2})	100 hours / 300 cycles (10 mA cm^{-2})	17
FeNi@NC-900	1.4	119	830.1 (10 mA cm^{-2})	70 hours (10 mA cm^{-2})	18
$FeNi_3$@NWC	1.47	143	805 (5 mA cm^{-2})	800 cycles (5 mA cm^{-2})	19
FeNi-NCS-2	1.43	109.8	639.71 (20 mA·cm^{-2})	130 cycles (10 mA cm^{-2})	20

Supplementary References

1. Y. Y. Wang, Y. P. Gao, L. X. Ma, Y. Z. Xue, Z. H. Liu, H. L. Cui, N. Zhang and R. B. Jiang, Atomically Dispersed Fe-N_4 Sites and NiFe-LDH Sub-Nanoclusters as an Excellent Air Cathode for Rechargeable Zinc-Air Batteries, *ACS Appl. Mater. Interfaces*, 2023, **15**, 16732-16743.
2. X. F. Zhu, D. T. Zhang, C. J. Chen, Q. R. Zhang, R. S. Liu, Z. H. Xia, L. M. Dai, R. Amal and X. Y. Lu, Harnessing the interplay of Fe-Ni atom pairs embedded in nitrogen-doped carbon for bifunctional oxygen electrocatalysis, *Nano Energy*, 2020, **71**, 104597.
3. X. Chen, J. Pu, X. H. Hu, Y. C. Yao, Y. B. Dou, J. J. Jiang and W. J. Zhang, Janus Hollow Nanofiber with Bifunctional Oxygen Electrocatalyst for Rechargeable Zn-Air Battery, *Small*, 2022, **18**, 2200578.
4. P. T. Liu, D. Q. Gao, W. Xiao, L. Ma, K. Sun, P. X. Xi, D. S. Xue and J. Wang, Self-Powered Water-Splitting Devices by Core-Shell NiFe@N-Graphite-Based Zn-Air Batteries, *Adv. Funct. Mater.*, 2018, **28**, 1706928.
5. X. Xie, H. Peng, K. J. Sun, X. F. Lei, R. Q. Zhu, Z. Zhang, G. F. Ma and Z. Q. Lei, Rational construction of $FeNi_3$/N doped carbon nanotubes for high-performance and reversible oxygen catalysis reaction for rechargeable Zn-air battery, *Chem. Eng. J.*, 2023, **452**, 139253.
6. B. Liu, B. W. Yuan, C. Wang, S. J. You, J. Liu, X. Meng, X. Q. Xu, Z. Cai, J. H. Xie and J. L. Zou, Highly-dispersed NiFe alloys in-situ anchored on outer surface of Co, N co doped carbon nanotubes with enhanced stability for oxygen electrocatalysis, *J. Colloid Interface Sci.*, 2023, **635**, 208-220.
7. T. Z. Li, Y. H. Chen, Z. H. Tang, Z. Liu and C. H. Wang, Palladium nanoparticles supported by metal-organic frameworks derived $FeNi_3C_x$ nanorods as efficient oxygen reversible catalysts for rechargeable Zn-Air batteries, *Electrochim. Acta*, 2019, **307**, 403-413.
8. G. L. Li, X. C. Xu, B. B. Yang, S. Cao, X. Y. Wang, X. D. Fu, Y. T. Shi, Y. Yan, X. D. Song and C. Hao, Micelle-template synthesis of a 3D porous FeNi alloy and nitrogen-codoped carbon material as a bifunctional oxygen electrocatalyst, *Electrochim. Acta*, 2020, **331**, 135375.
9. J. T. Ren, L. Chen, Y. S. Wang, W. W. Tian, L. J. Gao and Z. Y. Yuan, FeNi Nanoalloys Encapsulated in N-Doped CNTs Tangled with N-Doped Carbon Nanosheets as Efficient Multifunctional Catalysts for Overall Water Splitting and Rechargeable Zn-Air Batteries, *ACS Sustain. Chem. Eng.*, 2020, **8**, 223-237.
10. D. Z. Ren, J. Ying, M. L. Xiao, Y. P. Deng, J. H. Ou, J. B. Zhu, G. H. Liu, Y. Pei, S. Li, A. M. Jauhar, H. L. Jin, S. Wang, D. Su, A. P. Yu and Z. W. Chen, Hierarchically Porous Multimetal-Based Carbon Nanorod Hybrid as an Efficient Oxygen Catalyst for Rechargeable Zinc-Air Batteries, *Adv. Funct. Mater.*, 2020, **30**, 1908167.
11. H. Lei, Z. L. Wang, F. Yang, X. Q. Huang, J. H. Liu, Y. Y. Liang, J. P. Xie, M. S.

Javed, X. H. Lu, S. Z. Tan and W. J. Mai, NiFe nanoparticles embedded N-doped carbon nanotubes as high-efficient electrocatalysts for wearable solid-state Zn-air batteries, *Nano Energy*, 2020, **68**, 104293.

12. F. S. Farahani, M. S. Rahmanifar, A. Noori, M. F. El-Kady, N. Hassani, M. Neek-Amal, R. B. Kaner and M. F. Mousavi, Trilayer Metal-Organic Frameworks as Multifunctional Electrocatalysts for Energy Conversion and Storage Applications, *J. Am. Chem. Soc.*, 2022, **144**, 3411-3428.
13. D. Z. Ren, J. Ying, M. L. Xiao, Y. P. Deng, J. H. Ou, J. B. Zhu, G. H. Liu, Y. Pei, S. Li, A. M. Jauhar, H. L. Jin, S. Wang, D. Su, A. P. Yu and Z. W. Chen, Hierarchically Porous Multimetal-Based Carbon Nanorod Hybrid as an Efficient Oxygen Catalyst for Rechargeable Zinc-Air Batteries, *Adv. Funct. Mater.*, 2020, **30**, 1908167.
14. Y. L. Niu, X. Teng, S. Q. Gong and Z. F. Chen, A bimetallic alloy anchored on biomass-derived porous N-doped carbon fibers as a self-supporting bifunctional oxygen electrocatalyst for flexible Zn-air batteries, *J. Mater. Chem. A*, 2020, **8**, 13725-13734.
15. J. B. Tan, T. Thomas, J. X. Liu, L. Yang, L. H. Pan, R. Cao, H. J. Shen, J. C. Wang, J. Liu and M. H. Yang, Rapid microwave-assisted preparation of high-performance bifunctional Ni_3Fe/Co-N-C for rechargeable Zn-air battery, *Chem. Eng. J.*, 2020, **395**, 125151.
16. S. Liu, K. Dong, X. Lei, K. Sun, X. Xie, H. Peng and G. Ma, FeNi alloy embedded in three-dimensional nitrogen-doped porous carbon as bifunctional oxygen electrocatalysts for rechargeable Zn-air batteries, *Journal of Energy Storage*, 2024, **89**, 111862.
17. S. Zhang, L. Yang, T. Yang, Y. Song, M. Jia, J. Yang, Y. Liu, X. Zhou and J. Tang, Pomegranate-like structured FeNi-nanodots@FeNi LDH composite as a high performance bifunctional catalyst for oxygen electrocatalytic reactions in zinc-air batteries, *Composites Communications*, 2023, **44**, 101757.
18. S.-Q. Deng, Z. Zhuang, C.-A. Zhou, H. Zheng, S.-R. Zheng, W. Yan and J. Zhang, Metal-organic framework derived FeNi alloy nanoparticles embedded in N-doped porous carbon as high-performance bifunctional air-cathode catalysts for rechargeable zinc-air battery, *J. Colloid Interface Sci.*, 2023, **641**, 265-276.
19. Y. Wang, Y. Y. Liu, L. M. Zhou, P. X. Zhang, X. L. Wu, T. Liu, S. Mehdi, X. J. Guo, J. C. Jiang and B. J. Li, $Ni_3Fe/Ni_3Fe(OOH)_x$ dynamically coupled on wood-derived nitrogen doped carbon as a bifunctional electrocatalyst for rechargeable zinc-air batteries, *J. Mater. Chem. A*, 2023, **11**, 1894-1905.
20. Z. H. Yao, D. S. Chen, Y. T. Li, Q. Q. Lyu, J. Wang and Q. Zhong, MOF-derived multi-metal embedded N-doped carbon sheets rich in CNTs as efficient bifunctional oxygen electrocatalysts for rechargeable ZABs, *Int. J. Hydrog. Energy*, 2022, **47**, 984-992.